

## Structural properties of Bi<sub>2</sub>Te<sub>3</sub> and Bi<sub>2</sub>Se<sub>3</sub> topological insulators grown by molecular beam epitaxy on GaAs(001) substrates

X. Liu, D. J. Smith, J. Fan, Y.-H. Zhang, H. Cao et al.

Citation: *Appl. Phys. Lett.* **99**, 171903 (2011); doi: 10.1063/1.3655995

View online: <http://dx.doi.org/10.1063/1.3655995>

View Table of Contents: <http://apl.aip.org/resource/1/APPLAB/v99/i17>

Published by the [American Institute of Physics](#).

---

### Related Articles

Role of the substrate in the electrical transport characteristics of focused ion beam fabricated nanogap electrode  
*J. Appl. Phys.* **112**, 024310 (2012)

Tungsten silicide films for microwave kinetic inductance detectors  
*Appl. Phys. Lett.* **101**, 032601 (2012)

Thickness dependence oscillations of transport properties in thin films of a topological insulator Bi<sub>2</sub>Sb<sub>3</sub>  
*Appl. Phys. Lett.* **101**, 023108 (2012)

Resistivity in rough metallic thin films: A Monte Carlo study  
*J. Appl. Phys.* **112**, 013704 (2012)

Electron transport in discontinuous gold films and the effect of Coulomb blockade and percolation  
*J. Appl. Phys.* **111**, 123705 (2012)

---

### Additional information on *Appl. Phys. Lett.*

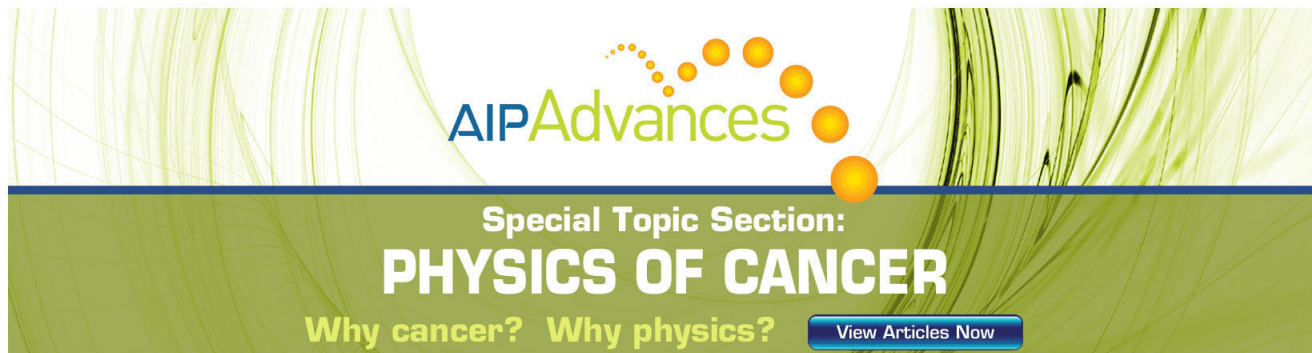
Journal Homepage: <http://apl.aip.org/>

Journal Information: [http://apl.aip.org/about/about\\_the\\_journal](http://apl.aip.org/about/about_the_journal)

Top downloads: [http://apl.aip.org/features/most\\_downloaded](http://apl.aip.org/features/most_downloaded)

Information for Authors: <http://apl.aip.org/authors>

## ADVERTISEMENT



**AIP Advances**

Special Topic Section:  
**PHYSICS OF CANCER**

Why cancer? Why physics? [View Articles Now](#)

# Structural properties of $\text{Bi}_2\text{Te}_3$ and $\text{Bi}_2\text{Se}_3$ topological insulators grown by molecular beam epitaxy on GaAs(001) substrates

X. Liu,<sup>1,a)</sup> D. J. Smith,<sup>2</sup> J. Fan,<sup>2,3</sup> Y.-H. Zhang,<sup>3,4</sup> H. Cao,<sup>5</sup> Y. P. Chen,<sup>5</sup> J. Leiner,<sup>1</sup> B. J. Kirby,<sup>6</sup> M. Dobrowolska,<sup>1</sup> and J. K. Furdyna<sup>1</sup>

<sup>1</sup>Department of Physics, University of Notre Dame, Notre Dame, Indiana 46556, USA

<sup>2</sup>Department of Physics, Arizona State University, Tempe, Arizona 85287, USA

<sup>3</sup>Center for Photonics Innovation, Arizona State University, Tempe, Arizona 85287, USA

<sup>4</sup>School of Electrical, Computer and Energy Engineering, Arizona State University, Tempe, Arizona 85287, USA

<sup>5</sup>Department of Physics, Purdue University, West Lafayette, Indiana 47907, USA

<sup>6</sup>Center for Neutron Research, NIST, Gaithersburg, Maryland 20899, USA

(Received 20 July 2011; accepted 4 October 2011; published online 24 October 2011)

Thin films of  $\text{Bi}_2\text{Te}_3$  and  $\text{Bi}_2\text{Se}_3$  have been grown on deoxidized GaAs(001) substrates using molecular beam epitaxy. Cross-sectional transmission electron microscopy established the highly parallel nature of the Te(Se)-Bi-Te(Se)-Bi-Te(Se) quintuple layers deposited on the slightly wavy GaAs substrate surface and the different crystal symmetries of the two materials. Raman mapping confirmed the presence of the strong characteristic peaks reported previously for these materials in bulk form. The overall quality of these films reveals the potential of combining topological insulators with ferromagnetic semiconductors for future applications. © 2011 American Institute of Physics. [doi:10.1063/1.3655995]

Recent photoemission measurements of the surfaces of topological insulators (TIs) such as  $\text{Bi}_{1-x}\text{Sb}_x$ ,  $\text{Bi}_2\text{Te}_3$  and  $\text{Bi}_2\text{Se}_3$  have confirmed that a conducting surface state with an odd number of Dirac points exists in these materials.<sup>1</sup> Theoretical models of topological insulators have predicted that this surface state should be robust and “topologically protected.”<sup>1</sup> Moreover, this conducting state is naturally spin-polarized, which opens up interesting opportunities for possible applications in spintronics.<sup>2</sup> The growth of such topological insulators by molecular beam epitaxy (MBE) is especially attractive because of the possibility to avoid defect formation by controlling the growth conditions. Efforts to fabricate TI thin films by MBE have included growth of  $\text{Bi}_2\text{Te}_3$  on substrates of Si(111),<sup>3,4</sup> and growth of  $\text{Bi}_2\text{Se}_3$  on substrates of graphene,<sup>3</sup> Si(111),<sup>5,6</sup> as well as GaAs(111).<sup>7</sup> Because representative spintronic materials, such as GaMnAs, are easily grown on GaAs (001) substrates,<sup>8</sup> and Fe films of very high crystalline perfection can also be grown on GaAs (001) or (110) substrates,<sup>9</sup> we are actively pursuing MBE growth of  $\text{Bi}_2\text{Te}_3$ ,  $\text{Bi}_2\text{Se}_3$  and their alloys on GaAs (001) substrates, with a goal to combine these electronic materials into multifunctional device configurations in the future. We demonstrate here that MBE growth of pseudo-hexagonal  $\text{Bi}_2\text{Te}_3$  and  $\text{Bi}_2\text{Se}_3$  thin films can also be achieved on GaAs (001) substrate despite the very different crystal symmetries along the film growth direction.

The  $\text{Bi}_2\text{Te}_3$  and  $\text{Bi}_2\text{Se}_3$  films were grown using a dual-chamber MBE system, with the growth process being monitored *in situ* by reflection-high-energy electron diffraction (RHEED). The growth sequence was usually as follows. First, the epi-ready GaAs (001) semi-insulating substrates were heated up to 600 °C for surface deoxidation. This deoxidation process was done either in the II–VI MBE chamber,

which was also equipped with high purity Bi, Te, and Se evaporators or, alternatively, in the III–V MBE chamber by depositing a 100-nm GaAs buffer layer on the deoxidized GaAs substrate, which was then transferred via an ultrahigh-vacuum load-lock assembly into the II–VI MBE chamber. The TI growth was initiated by the deposition of a sequence of either Te-Bi-Te-Bi-Te or Se-Bi-Se-Bi-Se atomic layers at room temperature. During this process, the  $(2 \times 4)$  RHEED pattern disappeared, indicating that an amorphous film had been deposited. The substrate was then gradually heated to about 300 °C to anneal the film, and a streaky RHEED pattern shown in Fig. 1 became visible, indicating that a quintuple layer (QL) of TI film had been formed.<sup>5</sup> It is important to note that the RHEED pattern showed recurrences six times during each rotation of the substrate, which confirms the *c*-axis growth of the pseudo-hexagonal TI films, with the *a*-axis lying along either the [110] or the  $[1\bar{1}0]$  direction of the GaAs (001) substrate. Two types of RHEED patterns were observed in this stage, depending on the length of annealing

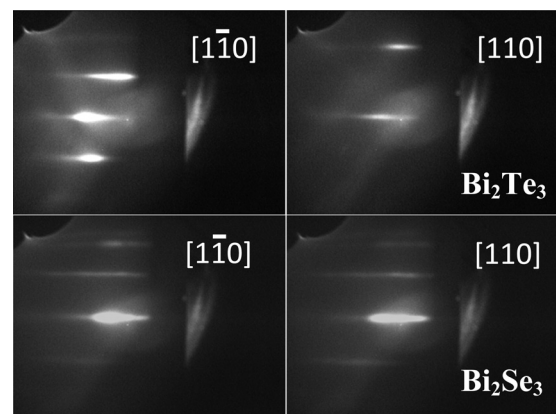


FIG. 1. RHEED patterns observed for two specific orientations of GaAs (001) substrate during MBE growth of (a)  $\text{Bi}_2\text{Te}_3$  and (b)  $\text{Bi}_2\text{Se}_3$ .

<sup>a)</sup> Author to whom correspondence should be addressed. Electronic mail: xliu2@nd.edu.

time. As shown in Fig. 1(a), usually observed in  $\text{Bi}_2\text{Te}_3$  case (QL of  $\text{Bi}_2\text{Te}_3$  usually survives for a longer annealing time than  $\text{Bi}_2\text{Se}_3$ ), longer annealing times yielded an unreconstructed pattern with distinct features observed for GaAs [110] and  $[\bar{1}\bar{1}0]$  directions, respectively. We attribute this to the hexagonal surface symmetry of the TI layer. On the other hand, short annealing times yielded the same RHEED patterns for both GaAs [110] and  $[\bar{1}\bar{1}0]$  directions, as shown in Fig. 1(b), which is often observed for  $\text{Bi}_2\text{Se}_3$ . Note that the RHEED pattern is actually a combination of the two distinct patterns seen on the [110] and  $[\bar{1}\bar{1}0]$  directions in the long annealing case. We therefore attribute this to the coexistence of two types of hexagonal surfaces perpendicular to each other. The MBE growth of  $\text{Bi}_2\text{Te}_3$  and  $\text{Bi}_2\text{Se}_3$  was then performed under the condition of  $T_{\text{Te}}$  (or  $T_{\text{Se}})$  <  $T_{\text{substrate}}$  ( $300^\circ\text{C}$ ) <  $T_{\text{Bi}}$  ( $500^\circ\text{C}$ ) with a Se(or Te):Bi beam equivalent pressure ratio ranging from 15:1 to 25:1. While no notable differences were observed for the growth of  $\text{Bi}_2\text{Te}_3$  and  $\text{Bi}_2\text{Se}_3$  when carried out on substrates with or without the GaAs buffer layer, the results described here refer only to TI films grown without the buffer layers. The TI thin films were grown layer-by-layer, with typical growth rates in this work of 2 QL/min, as characterized by RHEED oscillations (data not shown). RHEED patterns shown in Fig. 1 were maintained throughout the whole growth process. It should be emphasized that the same kind of growth is also observed on the Ga-rich GaAs (001) surfaces, i.e., surfaces with a  $(4 \times 6)$  RHEED pattern. We therefore attribute the growth of pseudo-hexagonal  $\text{Bi}_2\text{Te}_3$  and  $\text{Bi}_2\text{Se}_3$  on the GaAs (001) substrates to the weak Van der Waals coupling between the substrate and the TI films, leading to immediate strain relaxation as the interface is forming.<sup>3-7</sup>

The film thicknesses were determined *ex situ* through model-fitting<sup>10</sup> of the specular x-ray reflectivity (XRR), as shown by the example (thickness  $\sim 68$  nm) in Fig. 2. These thickness values were in reasonable agreement with the growth rates that were estimated *in situ* from RHEED oscillations. The standard deviation of film thickness obtained by fitting the XRR data was about 2.3 nm (3% of thickness), which suggests the root-mean-square roughness average (RMA) will be of the same order as that reported for the TI films of comparable thickness grown on other substrates.<sup>4</sup>

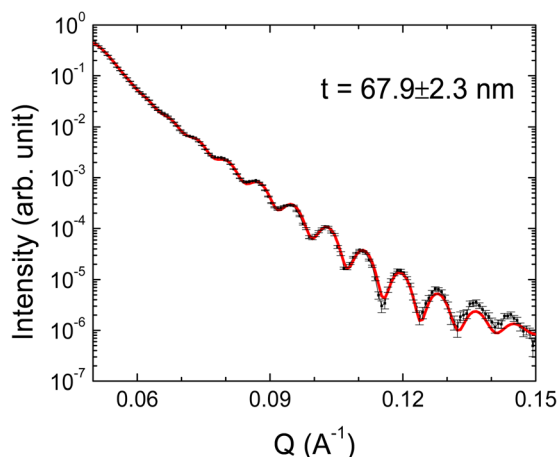


FIG. 2. (Color online) Model-fitted specular x-ray reflectivity of the  $\text{Bi}_2\text{Te}_3$  film, used for estimating the film thickness. Error bars correspond to  $\pm 1\sigma$ .

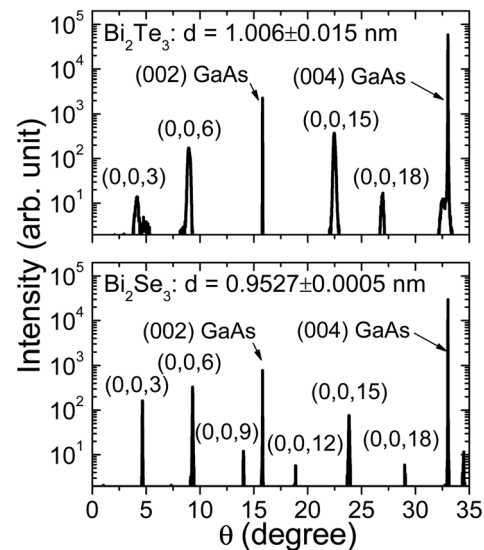


FIG. 3. X-ray diffraction patterns obtained from (a) 233-nm-thick  $\text{Bi}_2\text{Te}_3$  film and (b) 130-nm-thick  $\text{Bi}_2\text{Se}_3$  film grown by MBE on GaAs(001) substrate.

The overall crystallinity of the TI films was initially evaluated by high resolution x-ray diffraction (HR-XRD) using the Cu  $K_{\alpha 1}$  radiation line. Figure 3 shows XRD patterns that were obtained from: (a) a 233-nm-thick  $\text{Bi}_2\text{Te}_3$  film and (b) a 180-nm-thick  $\text{Bi}_2\text{Se}_3$  film, respectively. Strong reflections only from  $\{003\}$ -type lattice planes are visible, which is indicative of the highly pronounced  $c$ -axis growth of the film. The full-width-half-maximum for the (0,0,6) plane indicates that the crystallinity of  $\text{Bi}_2\text{Se}_3$  was considerably better than that of  $\text{Bi}_2\text{Te}_3$  (108 versus 763 s). The QL thicknesses were calculated from the XRD data, giving  $d_{\text{QL}} = 1.006 \pm 0.015$  nm for  $\text{Bi}_2\text{Te}_3$  and  $d_{\text{QL}} = 0.9527 \pm 0.0005$  nm for  $\text{Bi}_2\text{Se}_3$ , respectively (uncertainties correspond to  $1\sigma$ ). Both values are consistent with the values of 1.016 nm for the bulk  $\text{Bi}_2\text{Te}_3$  (Ref. 11) and 0.9545 nm for bulk  $\text{Bi}_2\text{Se}_3$ .<sup>12</sup>

The microstructure of the films was determined using cross-section transmission electron microscopy (XTEM). Samples were prepared for TEM examination using standard mechanical polishing and argon-ion-milling, with the sample held at liquid-nitrogen temperature during the latter process in order to avoid unintentional ion-milling artifacts. Gentle handling was necessary because the TI films had a tendency to peel away from the substrate during the preparation procedure, consistent with weak bonding between the TI films and the substrate. Figure 4(a) is an XTEM image showing a region of the  $\text{Bi}_2\text{Se}_3$  film close to the GaAs substrate surface. Despite the slightly wavy surface of the epi-ready GaAs substrate, highly parallel layers are clearly visible in the  $\text{Bi}_2\text{Se}_3$  film, suggesting that the high crystal quality is achieved by an internal self-correction process that is occurring as the growth proceeds. Figure 4(b) shows an enlarged view of the  $\text{Bi}_2\text{Se}_3/\text{GaAs}$  interface, which illustrates the pronounced planarity of the  $\text{Bi}_2\text{Se}_3$  lattice planes even in close proximity to the undulating GaAs surface. In addition, atomically sharp image of XTEM shows no dislocations and accumulated strain immediately above GaAs, despite the symmetry mismatch between the TI films and the GaAs (001) surface. This



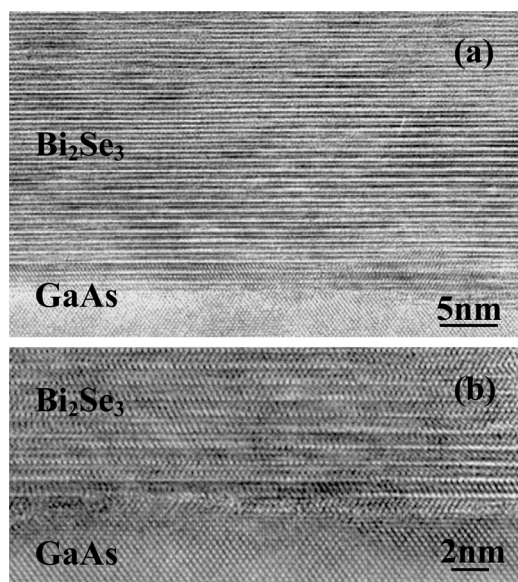


FIG. 4. Transmission electron microscopy (TEM) images showing cross sections of topological insulator  $\text{Bi}_2\text{Se}_3$  grown by MBE on a deoxidized  $\text{GaAs}(001)$  substrate.

observation undoubtedly confirms the rapid relaxation of strain at the interface, which is similar to what is observed on graphene and Si.<sup>3-7</sup> We attribute such unique feature to the weak van der Waals coupling between adjacent QLs in the TI films. TEM images also confirmed that the  $a$ -axis of the pseudo-hexagonal TI films lies along either the  $[110]$  or the  $[1\bar{1}0]$  direction of the  $\text{GaAs}(001)$  substrate.

Micro Raman spectroscopy with a 532-nm excitation laser (power  $\sim 0.8$  mW) was also performed. The results, shown in Fig. 5, reveal three of the characteristic peaks for  $\text{Bi}_2\text{Se}_3$  [at  $\sim 71$   $\text{cm}^{-1}$  ( $A^1_{1g}$ ),  $131$   $\text{cm}^{-1}$  ( $E^2_g$ ), and  $174$   $\text{cm}^{-1}$  ( $A^2_{1g}$ )], and two of the characteristic peaks for  $\text{Bi}_2\text{Te}_3$  [at  $\sim 102$   $\text{cm}^{-1}$  ( $E^2_g$ ) and  $134$   $\text{cm}^{-1}$  ( $A^2_{1g}$ )]. The peaks observed in these two TI materials are consistent with the lattice vibration modes reported earlier.<sup>13</sup> Moreover, Raman mapping showed that the positions of these Raman peaks measured within a scan area of  $15\ \mu\text{m} \times 15\ \mu\text{m}$  vary spatially by less than  $\sim 1$   $\text{cm}^{-1}$ , indicating a good uniformity of the films.

In summary, even though there is mismatch between the hexagonal lattices of  $\text{Bi}_2\text{Te}_3$  and  $\text{Bi}_2\text{Se}_3$  topological insulators and the cubic symmetry of the  $\text{GaAs}(001)$  surface, we have grown high quality epitaxial films of  $\text{Bi}_2\text{Te}_3$  and  $\text{Bi}_2\text{Se}_3$  on  $\text{GaAs}(001)$  substrates. The films are highly uniform and the crystallinity is comparable to that of films grown on substrates with hexagonal surface structure. Future studies of  $\text{Bi}_2\text{Te}_3$  and  $\text{Bi}_2\text{Se}_3$  grown on  $\text{GaAs}(001)$  substrates should contribute towards a better knowledge of MBE growth of topological insulators, as well as opening up the opportunity for future spin-based devices that combine topological insulators with ferromagnetic semiconductors.

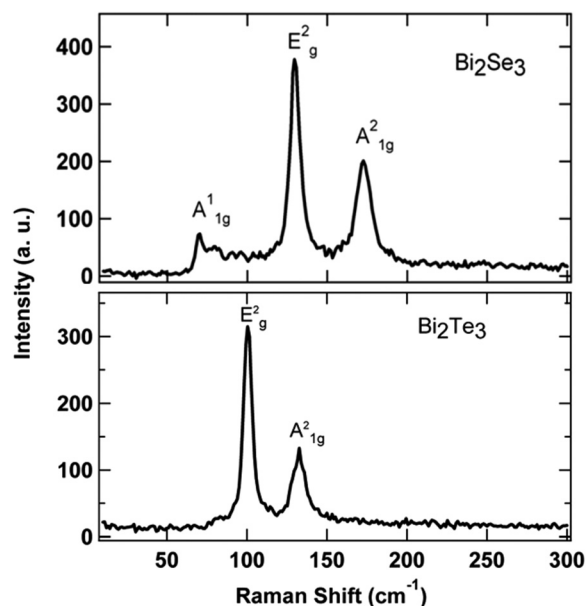


FIG. 5. Representative Raman spectra measured in MBE films of: (a)  $\text{Bi}_2\text{Te}_3$  and (b)  $\text{Bi}_2\text{Se}_3$ . The film (a) is 136 nm thick and the film (b) is 150 nm thick.

This work was supported by NSF Grant DMR10-05851 for ND; for ASU an NSF grant, contract number 1002114 and an AFOSR Grant number FA9550-10-1-0129; Y.P.C. acknowledges support from DARPA MESO program. The authors acknowledge use of facilities in the John M. Cowley Center for High Resolution Electron Microscopy at Arizona State University and the x-ray reflectometer at the NIST Center for Neutron Research.

<sup>1</sup>M. Z. Hasan and C. L. Kane, *Rev. Mod. Phys.* **82**, 3045 (2010).

<sup>2</sup>S.-C. Zhang, *Physics* **1**, 6 (2008).

<sup>3</sup>X. Chen, X.-C. Ma, K. He, J.-F. Jia, and Q.-K. Xue, *Adv. Mater.* **23**, 1162 (2011).

<sup>4</sup>J. Krumwain, G. Mussler, S. Borisova, T. Stoica, L. Plucinski, C. M. Schneider, and D. Grützmacher, *J. Cryst. Growth* **324**, 115 (2011).

<sup>5</sup>G. Zhang, H. Qin, J. Teng, J. Guo, Q. Guo, X. Dai, Z. Fang, and K. Wu, *Appl. Phys. Lett.* **95**, 053114 (2009).

<sup>6</sup>H. D. Li, Z.Y. Wang, X. Guo, T. L. Wong, N. Wang, and M. H. Xie, *Appl. Phys. Lett.* **98**, 043104 (2011).

<sup>7</sup>A. Richardella, D. M. Zhang, J. S. Lee, A. Koser, D. W. Rench, A. L. Yeats, B. B. Buckley, D. D. Awschalom, and N. Samarth, *Appl. Phys. Lett.* **97**, 262104 (2010).

<sup>8</sup>J. Sadowski, R. Mathieu, P. Svedlindh, J. Z. Domagała, J. Bak-Misiuk, K. Świątek, M. Karlsteen, J. Kanski, L. Ilver, H. Åsklund, and U. Södervall, *Appl. Phys. Lett.* **78**, 3271 (2001).

<sup>9</sup>J. J. Krebs, B. T. Jonker, and G. A. Prinz, *J. Appl. Phys.* **61**, 2596 (1987).

<sup>10</sup>P. A. Kienzle, M. Doucet, D. J. McGillivray, K. V. O'Donovan, N. F. Berk, and C. F. Majkrzak, NCTR Reflectometry Software. Available at the NIST Center for Neutron Research, <http://www.ncnr.nist.gov/reflpak>.

<sup>11</sup>J. O. Jenkins, J. A. Rayne, and J. R. W. Ure, *Phys. Rev. B* **5**, 3171 (1972).

<sup>12</sup>S. Nakajima, *J. Phys. Chem. Solids* **24**, 479 (1963).

<sup>13</sup>W. Richter, H. Kohler, and C. R. Becker, *Phys. Status Solidi. B* **84**, 619 (1977).